07,13

The effect of Sr concentration on the crystal and magnetic structures of $La_{1-x}Sr_xFeO_{3-\gamma}$ orthoferrite

© V. Sedykh[1], O. Rybchenko[1], A. Dmitriev[2], V. Kulakov[1], A. Gapochka[3], V. Rusakov[3]

[1] Osipyan Institute of Solid State Physics, Russian Academy of Sciences, Chernogolovka, Moscow District, Russia
[2] Federal Research Center of Problems of Chemical Physics and Medical Chemistry, Russian Academy of Sciences, Chernogolovka, Moscow District, Russia
[3] Lomonosov Moscow State University, Moscow, Russia

E-mail: sedykh@issp.ac.ru

Received September 2, 2024
Revised September 17, 2024
Accepted October 18, 2024

The structural and magnetic features of substituted $La_{1-x}Sr_xFeO_{3-\gamma}$ have been studied, in both synthesized and vacuum−annealed samples, depending on the Sr content (for $x = 0.33$ and 0.50), using X-ray diffraction, Mössbauer spectroscopy and magnetic measurements. It has been shown that in the as−prepared samples, the volume of the pseudocubic perovskite cell decreased and the number of vacancies and Fe^{4+} ions increased with an increase in the Sr concentration. The Néel temperatures were determined for two compositions of the compound: $T_N \approx 233$ K for the $La_{0.5}Sr_{0.5}FeO_{3-\gamma}$ sample and $T_N \approx 385$ K for the $La_{0.67}Sr_{0.33}FeO_{3-\gamma}$ sample. The contributions of Fe^{3+} ions with different local environments were redistributed under vacuum annealing. That led to changes in the J_F/J_{AF} ratio, a shift in the balance towards increasing antiferromagnetism, a noticeable increase in the Néel temperature T_N, and a decrease in the width of the magnetic hysteresis loops and the magnetization value.

Keywords: substituted lanthanum ferrites, orthoferrites, Fe valence states, oxygen vacancies, X-ray diffraction analysis, Mössbauer spectroscopy, magnetization.

DOI: 10.61011/PSS.2024.11.60100.229

1. Introduction

Due to unusual electrical, magnetic and catalytic properties, perovskite $R_{1-x}A_xFeO_{3-\gamma}$ orthoferrites, where R is a rare earth element, A is Ba, Ca, and Sr, are promising materials in various fields, for example, as electrode materials for fuel cells, catalysts, chemical sensors, optoelectronic devices, magnetic memory devices, etc. [1,2]. Recently it has been published researches indicating the powerful antibacterial properties of these compounds, associated with the presence of oxygen vacancies in the lattice [3]. Ions of transition metal Fe in these systems have mixed valence states, Fe^{3+} and Fe^{4+}, which results from the substitution of divalent ions (A) for a trivalent element (R) [4].

For $La_{1-x}A_xFeO_{3-\gamma}$ compounds, there is a relationship between the proportion of the substituent divalent element, oxygen content, and the quantitative ratio between the Fe^{3+} and Fe^{4+} valence states. The standard procedure for orthoferrite synthesis using the sol−gel method involves the participation of oxygen from the air in this process. High−temperature annealing in different atmospheres (air, oxygen, and vacuum) also affects the oxygen content in the lattice and the valence state of Fe ions. This ultimately determines the structure of the compound and its physical properties. In addition, the difference between the ionic radii of La and the substituent element can play an important role in the formation of a particular crystal lattice. It is extremely difficult to distinguish the influence of each of the changing parameters; therefore it is necessary to minimize their number. In this regard, a series of studies were carried out on the as−prepared $La_{1-x}Sr_xFeO_{3-\gamma}$ ferrites with fixed ratios of the number of La/Sr ions and on the samples annealed in vacuum in a certain temperature range. In the synthesized (as−prepared) samples, the number of Fe^{4+} ions is maximum, while the number of oxygen vacancies is minimum [5–12]. Vacuum annealing reduces the number of oxygen ions and, accordingly, Fe^{4+} ions. It is possible to select a vacuum annealing temperature at which all Fe^{4+} ions transfer to Fe^{3+} and the removal of oxygen from the lattice ends.

Magnetic properties in the basic unsubstituted lanthanum ferrite, $LaFeO_3$, result from superexchange interactions involving $3d$ orbitals of Fe^{3+} ions and p orbitals of oxygen [13]. According to Goodenough's theory [14], the superexchange interaction $Fe^{3+}-O^{2-}-Fe^{3+}$ between Fe^{3+} ions is antiferromagnetic, and is stronger than that between Fe^{4+} and Fe^{3+} ions. The presence of Fe^{4+} ions in the substituted $La_{1-x}Sr_xFeO_{3-\gamma}$ lanthanum ferrite weakens the superexchange interaction, which lowers the Néel temperature T_N [15,16].

Based on the aforesaid, the study of the influence of each variable parameter on certain properties of orthoferrites, as

well as the investigation of interrelated processes occurring in the structure of substituted orthoferrites at the local level and their correlation with the magnetic properties of these compounds is important both from the viewpoint of both science and application.

The present work aimed to summarize the data on interrelated processes occurring during vacuum annealing in $La_{1-x}Sr_xFeO_{3-\gamma}$ compounds with a fixed Sr concentration of 33% and 50%, determine the dependence of these processes on the fraction of divalent ions (Sr).

2. Materials and methods

The as−prepared polycrystalline $La_{0.67}Sr_{0.33}FeO_{3-\gamma}$ (Sr33) and $La_{0.5}Sr_{0.5}FeO_{3-\gamma}$ (Sr50) samples were synthesized in the air by the sol−gel method at 1100°C for 20 h using Sr, Fe and La nitrates in a stoichiometric proportion and glycine as starting reagents. The details of the synthesis were described in [5]. After the synthesis, the samples and the furnace were slowly cooled down to room temperature. Then the samples were annealed in vacuum (10^{-3} Torr) at the temperatures of 200−650°C for 4 h to vary the oxygen content.

The structural characterization of the polycrystalline samples was carried out at room temperature (RT) by X-ray powder diffraction on a Rigaku SmartLab SE diffractometer using CuK_α radiation. The Powder Cell 2.4 and Match3 software packages were used for the phase analysis and determination of the structural parameters.

Mössbauer measurements of the polycrystalline samples were performed at RT and 85 K on an SM 1101 spectrometer operating in a constant acceleration mode. The radioactive source was ^{57}Co (Rh). The spectra were fitted and analyzed using model fitting and reconstruction of the distribution of hyperfine spectral parameters by the SpectrRelax program [17].

The temperature dependencies of magnetic moment $M(T)$ and magnetic field strength $M(H)$ were measured using a vibrating sample magnetometer of a CFMS multifunctional cryomagnetic measuring unit (Cryogenic Ltd, UK). The $M(T)$ dependencies were measured in the ZFC (the sample was precooled in zero magnetic field) and FC (the sample was precooled in a magnetic field $H = 10$ kOe) modes within the temperature range $T = 2-400$ K in a magnetic field $H = 1$ kOe. The $M(H)$ dependencies were measured in the form of magnetic hysteresis loops at $T = 2$ and 300 K in magnetic fields with strength of up to 50 kOe.

3. Results and discussion

3.1. X−ray diffraction data

The X−ray diffraction data for $SrFeO_{3-\gamma}$ and substituted $La_{1-x}Sr_xFeO_{3-\gamma}$ at different fixed La/Sr ratios for as−prepared and annealed in vacuum samples were given in our previous papers [5–12]. In this study, the structure of ferrites was analyzed depending on the Sr concentration. For each ratio La/Sr, two equilibrium states were considered — the as−prepared ferrite, synthesized by the sol−gel method and that annealed in vacuum at 650°C. This annealing temperature was chosen because such heat treatment leads to a complete transition of Fe^{4+} to Fe^{3+} and stabilization of the equilibrium oxygen content in all studied compositions. Some of the data will be given for a range of ferrites from $SrFeO_{3-\gamma}$ to $LaFeO_3$. The detailed study of the structure, including that at the local level using Mössbauer spectroscopy, was carried out for two samples with the Sr concentrations $x = 0.33$ and 0.50 (Sr33 and Sr50). The changes in them under vacuum annealing were sequential and continuous in contrast to the $La_{0.33}Sr_{0.67}FeO_{3-\gamma}$ (Sr67) and $SrFeO_{3-\gamma}$ compositions. In the last two compositions, depending on the oxygen content, a series of phases with different structures was formed [5–7].

As our data have shown, the as−prepared Sr33 sample has an orthorhombic structure (space group $Pbnm$, JCPDS 01-089-1269) [11]. The diffraction pattern is described a little better when a small amount of the rhombohedral phase $R\bar{3}c$ is added. Both phases have a perovskite−like structure and close crystal lattice volumes per formula unit, V/Z ($Z = 4$ for $Pbnm$, and $Z = 6$ for $R\bar{3}c$). However superimposing the diffraction lines and their significant widening do not allow the determination of the parameters of these phases and their quantitative relation with sufficient reliability. Therefore the unit cell volume V/Z was calculated using the single-phase approximation ($Pbnm$). After vacuum annealing at 650°C, the sample becomes single−phase with an orthorhombic structure. The lattice parameters and unit cell volume change monotonously under vacuum annealing at different temperatures.

The as−prepared Sr50 sample has a rhombohedral structure $R\bar{3}c$ (JCPDS 01-089-1269); its unit cell is a slightly distorted cubic one. The rhombohedral distortion of the unit cell is reduced under vacuum annealing, and the sample annealed at 650°C has a cubic structure $Pm\bar{3}m$ ($V/Z = 1$). Figure 1 shows the dependence of the perovskite cell volume on the vacuum annealing temperature T_{ann} for the Sr33 and Sr50 samples. Figure 2 illustrates the dependence of the unit cell volume V/Z on the Sr concentration in the as−prepared and annealed samples. For comparison, the data for $SrFeO_{3-\gamma}$, $LaFeO_3$, and the substituted lanthanum ferrite with $x = 0.67$ (Sr67) are also presented in Figure 2 [5,7]. There is a general tendency to decrease volume with an increase in the Sr concentration. For the as−prepared samples, the dependence has a continuous character, whereas the volume of the annealed samples increases abruptly when Sr50 transfers to Sr67. This is due to significant changes in the structure of Sr67 and $SrFeO_{3-\gamma}$ samples under vacuum annealing with the formation of the vacancy-ordered layered phases: $LaSr_2Fe_3O_8$ and brownmillerite $SrFeO_{2.5}$ phases. These phases have a fundamental difference in the local structure of the lattice — the presence of a tetrahedral oxygen environment of Fe^{3+} ions along with an octahedral one [6]. These structures are

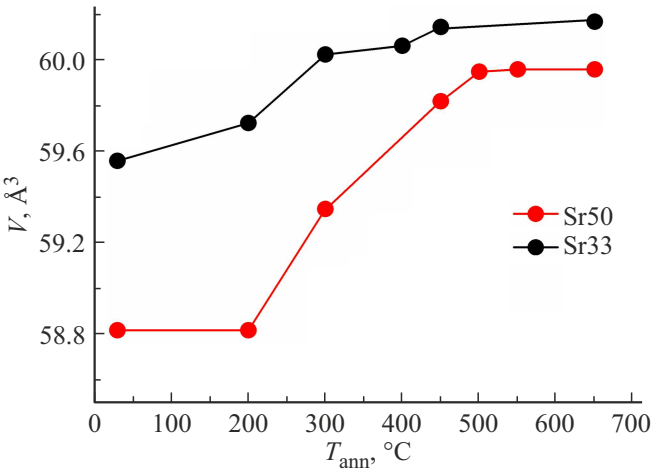

Figure 1. The dependence of the perovskite cell volume on a vacuum anntaling temperature Tann for the Sr50 and Sr33 samples. The drawn lines are guides for the eye.

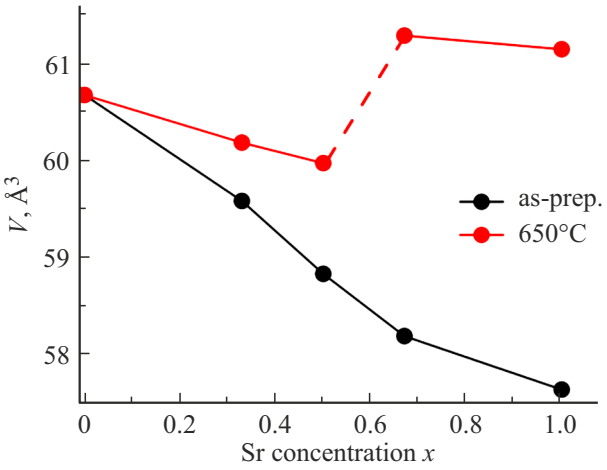

Figure 2. The dependence of the perovskite cell volume on the Sr concentration in the as–prepared samples and those annealed in vacuum at 650°C.

beyond the scope of this task, and are not discussed in detail in this work.

In the as–prepared ferrite samples, the unit cell volume V/Z decreases with an increase in the Sr concentration, in spite of the larger Sr^{2+} ionic radius as compared to the La^{3+} one [18]. Usually this fact is associated with the change in the valence state of Fe ions (from Fe^{3+} to Fe^{4+}) and with the difference between their ionic radii. The Fe^{4+} ionic radius (0.585 Å) is significantly smaller as compared to the Fe^{3+} one (0.645 Å), therefore the crystal lattice volume decreases when Sr is substituted for La and, accordingly, the Fe^{4+} ion fraction increases. In addition, an oxygen concentration decreases with an increase in Sr content.

With an increase in the Sr concentration up to 50%, the unit cell volume in the annealed samples also decreases linearly but not as sharply as in the as–prepared samples (Figure 2). One can suppose that in this case the decrease in the volume is assiciated with the change in the oxygen concentration only since alone Fe^{3+} ions are in the lattice of the samples annealed at 650°C.

3.2. Mössbauer data

The data on the valence states of Fe atoms in substituted $La_{1-x}Sr_xFeO_{3-\gamma}$ ferrites can be obtained using Mössbauer spectroscopy. The area of the Mössbauer subspectra is proportional to the number of the appropriate Fe valence states. The oxygen content of the samples can be estimated with a good accuracy when the number of the Fe valence states is known. The detailed Mössbauer studies of the samples with a fixed number of Sr ions, Sr50 and Sr33, were carried out in [9–12].

It follows from the values of the isomer shift δ of the RT Mössbauer spectra of the as–prepared Sr33 and Sr50 samples that, in addition to Fe^{3+}, a part of Fe ions is in an average-valence state, i.e. with a fractional oxidation degree between 3+ and 4+ [9,12]. This average–valence state of Fe ions is due to the fast (with a characteristic time of $< 10^{-8}$ s) electron transfer between Fe^{3+} and Fe^{4+} ions at room temperature; therefore, Fe^{4+} ions in substituted ferrites are not detected in the RT Mössbauer spectra [16,19,20]. An increase in the number of oxygen vacancies under vacuum annealing should lead to distortion of the oxygen environment of Fe ions and, therefore, to an increase in the quadrupole shift of the Mössbauer spectra. However, the average value of the quadrupole shift ε_{aver} is near zero. It can be assumed that oxygen ions due to their high mobility in these ferrites [21] are redistributed so that a more symmetrical oxygen environment of Fe ions is created.

Since the Fe valence states of the Sr33 and Sr50 samples could not be detected in a pure form from the RT Mössbauer spectra, the 85 K Mössbauer measurements were carried out [10–12]. The principal hyperfine parameters and relative areas (I) of the subspectra of Fe^{3+} and Fe^{4+} ions for the Sr33 and Sr50 samples are listed in Table 1.

The model fitting results showed that the spectra consist of several subspectra in the form of Zeeman sextets. One of them with the smallest isomer shift and a hyperfine magnetic field can be attributed to Fe^{4+} ions, while the others can be attributed to Fe^{3+} ions. The presence of several subspectra for Fe^{3+} ions is due to the different numbers of oxygen vacancies and Fe^{4+} ions in the nearest environment of Fe^{3+} ions, i.e. a heterogeneous local environment is formed. A Fe^{4+} ion weakens the superexchange interaction $Fe^{3+}–O^{2-}–Fe^{3+}$ in the nearest cation environment of a Fe^{3+} ion. An oxygen vacancy leads to the breaking of the superexchange interaction in the nearest anion environment of a Fe^{3+} ion. Both of them reduce the hyperfine magnetic field H_{hf} and change the isomer shift value for Fe^{3+} ions [22,23].

Assuming the recoil–free fraction for Fe^{3+} and Fe^{4+} to be the same, the number of Fe^{4+} ions ($y = I(Fe^{4+})$), oxygen vacancies $\gamma = (x-y)/2$, and oxygen anions $(3-\gamma)$ per

Table 1. Hyperfine parameters (isomer shift δ, quadrupole shift ε and magnetic field H_n) and relative areas (I) of the subspectra of the Fe^{3+} (averaged values) and Fe^{4+} ions in the 85 K experimental Mössbauer spectra of the as–prepared and annealed at 650°C $La_{1-x}Sr_xFeO_{3-\gamma}$ samples ($x = 0.33$ and 0.50)

X	T_{ann}	Fe	δ, mm/s	ε, mm/s	H_n, kOe	I, %
0.33	as–pr.	Fe^{3+}	0.385 ± 0.006	-0.011 ± 0.006	523.1 ± 0.5	83.3 ± 0.9
		Fe^{4+}	-0.083 ± 0.015	-0.013 ± 0.015	257.2 ± 0.2	16.7 ± 0.9
	650°C	Fe^{3+}	0.439 ± 0.004	-0.004 ± 0.003	548.3 ± 0.5	99.1 ± 0.8
		Fe^{4+}	-0.083	-0.013	257.2	0.9 ± 0.8
0.50	as–pr.	Fe^{3+}	0.393 ± 0.011	-0.009 ± 0.009	496.7 ± 4.0	74.5 ± 1.0
		Fe^{4+}	-0.062 ± 0.012	-0.028 ± 0.012	257.8 ± 0.9	25.5 ± 1.0
	650°C	Fe^{3+}	0.421 ± 0.008	-0.015 ± 0.005	540.7 ± 2.1	98.5 ± 1.0
		Fe^{4+}	-0.062	-0.028	257.8	1.5 ± 1.0

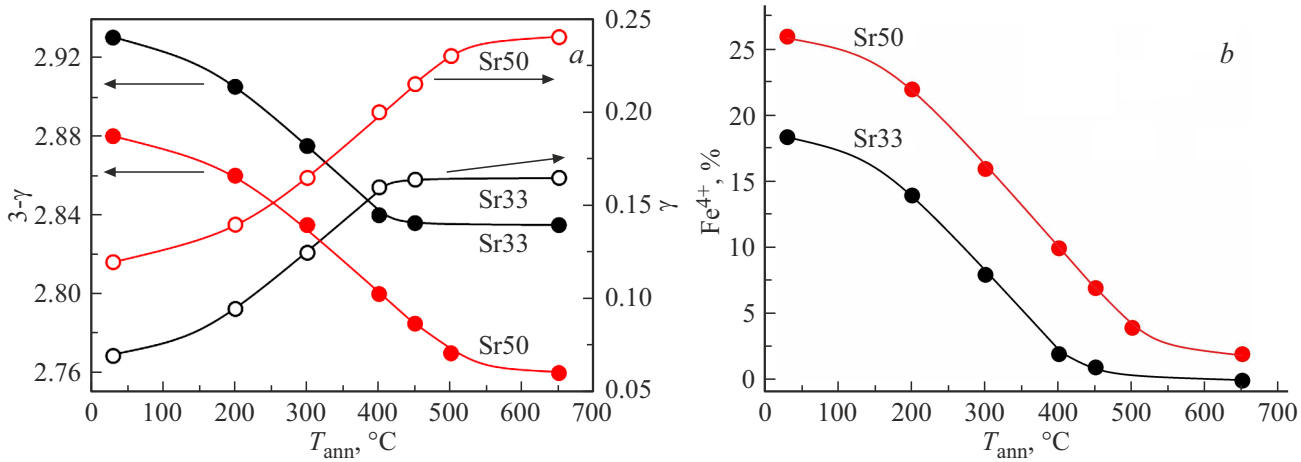

Figure 3. The T_{ann} dependence of the number of (a) oxygen ions ($3-\gamma$) and vacancies (γ) and (b) Fe^{4+} ions for Sr33 and Sr50. The drawn lines are guides for the eye.

formula unit can be determined from the relative areas of the subspectra of Fe ions, when the number of Sr^{2+} ions (x) is fixed. The numbers of Fe valence states and oxygen anions (oxygen vacancies) were determined in [10–12] for the as–prepared Sr33 and Sr50 samples and those annealed in vacuum at different temperatures (200–650°C) with fixed La/Sr ratios. Figure 3 shows the T_{ann} dependencies of the number of oxygen ions, vacancies, and Fe^{4+} ions the in Sr33 and Sr50 ferrites. Their initial data were taken from the works [5,7]. The as–prepared samples have a maximum number of Fe^{4+} ions and a minimum number of vacancies. As noted above, with an increase in the Sr concentration, the number of Fe^{4+} ions increases and the number of oxygen anions decreases. Under vacuum annealing, the number of oxygen anions and, accordingly, Fe^{4+} ions decreases, and the number of oxygen vacancies increases with an increase in T_{ann}. In this case all Fe^{4+} ions transfer to Fe^{3+}, the removal of oxygen from the lattice ends, and the number of oxygen vacancies is maximum at $T_{ann} = 650$°C.

Figure 4, a illustrates the change in the number of Fe^{4+} ions in the as–prepared samples as a function of the Sr concentration. The data for the Sr67 and $SrFeO_{3-\gamma}$ samples were taken from the works [5,7]. As it follows from the figure, the number of Fe^{4+} ions in the as–prepared samples increases linearly with an increase in the Sr concentration. Based on the Mössbauer data, $y \approx x/2$ and $\gamma \approx (x-x/2)/2 \approx x/4$. The dependence of the number of vacancies and oxygen ions on the Sr concentration in the as–prepared samples and those annealed at 650°C is shown in Figure 4, b. In this case, a linear dependence is observed. In the annealed samples (Fe^{4+} ions are absent), a decrease in the number of oxygen ions (and, accordingly, an increase in the number of vacancies) occurs faster with an increase in the Sr concentration. The reason is that only vacancies in the annealed samples participate

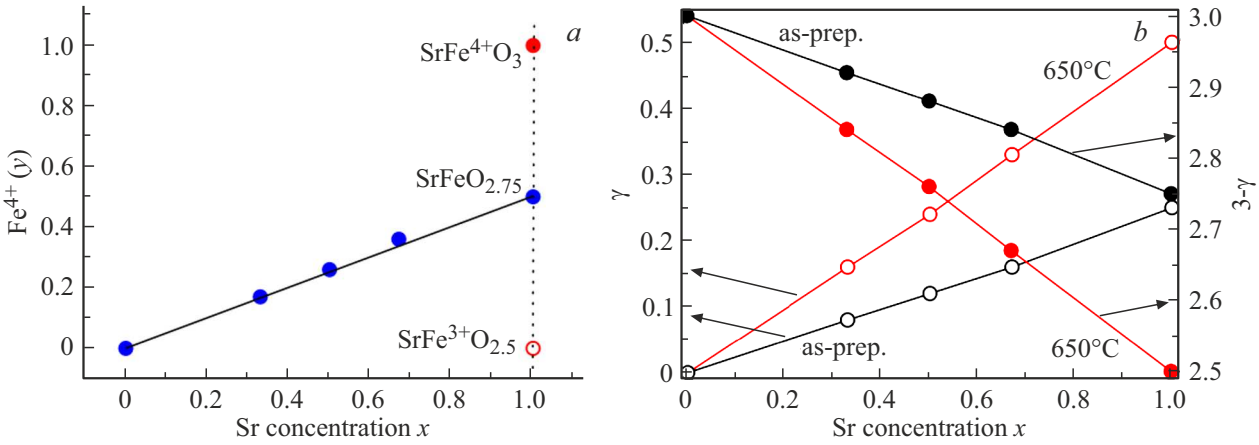

Figure 4. The Sr concentration dependence of the number of (a) Fe^{4+} (y) ions in the as−prepared samples and (b) oxygen ions and oxygen vacancies in the as−prepared and annealed in vacuum at 650°C samples.

in the process of compensating for the charge imbalance of the cation subsystem ($La^{3+}_{1-x}Sr^{2+}_x$) associated with Sr substitution for La.

The use of Mössbauer data enables not only calculating the average macroscopic characteristics of the compound, such as the fraction of Fe^{4+} and the number of oxygen ions, but also obtaining information on the structure at the local level. The dependence of the parameters of each individual subspectrum of Fe^{3+} ions on the number of Fe^{4+} ions and vacancies in the nearest Fe environment allows it to be associated with a specific version of this environment (with the number of broken or weakened exchange bonds), while the analysis of the areas of subspectra permits estimation of the quantitative distribution of these defects over the lattice. Let us introduce the number m, which is — the number of broken or weakened exchange bonds of a Fe^{3+} ion. The value $m = 0$ means that the Fe^{3+} ion in the nearest environment has all six $Fe^{3+}-O^{2-}-Fe^{3+}$ exchange bonds, i. e. there are no oxygen vacancies and Fe^{4+} ions. The T_{ann} dependence of the areas of the Fe^{3+} subspectra for the Sr33 and Sr50 samples for different m values was obtained in [10,12]. By using this data, it is possible to construct their dependence on the number m for the as−prepared Sr33 and Sr50 samples and those annealed at 650°C (Figure 5).

In the as−prepared samples, the area of the subspectra corresponding to the state $m = 0$ (there are no vacancies and Fe^{4+} ions in the nearest environment of the Fe^{3+} ion) is small: $\sim 18\%$ for the Sr33 sample and $\sim 13\%$ for the Sr50 sample. The subspectra with $m = 1$ for Sr33 and $m = 2$ for Sr50 have the maximum area ($\sim 40\%$ and $\sim 35\%$, respectively). This means that most Fe ions in the as−prepared samples have one or two defects in their local environment — a broken or a weakened bond. The subspectra of the samples annealed at 650°C have the maximum area at $m = 0$: $\sim 70\%$ for Sr33 and $\sim 60\%$ for Sr50. Their areas greatly decrease with an increase in the number m.

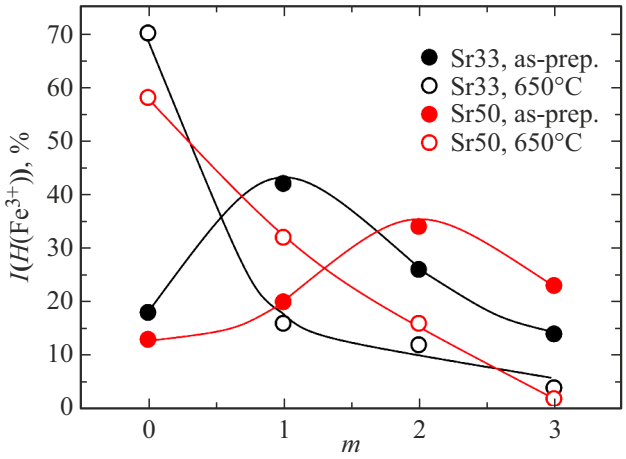

Figure 5. The dependence of the area $I\left(H(Fe^{3+})\right)$ of the subspectra on the number m for the as−prepared and annealed Sr33 and Sr50 samples.

Thus, the subspectra of Fe^{3+} ions with an octahedral oxygen environment, i. e., with $m = 0$, are the most intense in the annealed samples when there are neither Fe^{4+} ions nor oxygen vacancies in the nearest environment of Fe^{3+} ions. In general, the degree of distortion of the nearest environment of Fe ions for the Sr33 sample is smaller than for the Sr50 sample, which correlates with the number of oxygen vacancies in them.

3.3. Schematics of the processes under synthesis

For the $La_{1-x}Sr_xFeO_{3-\gamma}$ lanthanum ferrites, the substitution of Sr^{2+} for La^{3+} in the $LaFeO_3$ lattice leads to a decrease in the number of oxygen ions and the formation of vacant oxygen positions (defects) because of the necessary maintenance of the charge balance. Let us suppose that Fe ions are only in the 3+ oxidation state in the compound, as in $LaFeO_3$. Then, for such the

Table 2. The summary data on the number of vacancies (γ), oxygen ($3-\gamma$) and Fe^{4+} (y) ions, as well as the volume (V) per formula unit, for all the studied Sr33 and Sr50 samples, both as−prepared and annealed in vacuum at 650°C

Sample	γ	$3-\gamma$	Fe^{4+} (y)	V (Å^3)
Sr33 (as−prepared)	0.08	2.92	0.18	59.59
Sr50 (as−prepared)	0.12	2.88	0.26	58.82
Sr33 (650°C)	0.16	2.84	0	60.18
Sr50 (650°C)	0.24	2.76	0	59.96

Table 3. The summary data on changes in the number of vacancies ($\Delta\gamma$), oxygen ions ($\Delta(3-\gamma)$), Fe^{4+} ions (ΔFe^{4+}), and volume per formula unit (ΔV) with Sr variations (Sr33 → Sr50) and a change in vacuum annealing (as−prepared → 650°C)

Composition and annealing conditions		$\Delta\gamma$	$\Delta(3-\gamma)$	ΔFe^{4+} (Δy)	ΔV (Å^3)
Sr33 → Sr50	as−prepared	+0.04	−0.04	+0.08	−0.77
	650°C	+0.08	−0.08	0	−0.22
as−prepared → 650°C	Sr33	+0.08	−0.08	−0.18	+0.59
	Sr50	+0.12	−0.12	−0.26	+1.14

state, the oxygen concentration is quantitatively related to the proportion of Sr^{2+} ions, it decreases with an increase in the proportion of Sr^{2+}. Let's call this oxygen „basic"; its number is determined by the La^{3+}/Sr^{2+} ratio. This state of the $La_{1-x}Sr_xFeO_{3-\gamma}$ compound is observed in samples annealed in vacuum at a temperature of 650°C and having a minimum oxygen content.

It is known that iron is able to change its valence and form mixed valence states. In practice, during the synthesis of orthoferrites, the number of oxygen ions entering the lattice significantly exceeds the „base" level, and Fe^{3+} ions are partially oxidized to the Fe^{4+} state. The additional oxygen relative to the „base" one is in balance with Fe^{4+} and is uniquely associated with it by a simple quantitative relation. Let's call it a „variable". Then, the compound formula is written as

$$La^{3+}_{1-x}Sr^{2+}_{x}Fe^{3+}_{1-y}Fe^{4+}_{y}O^{2-}_{3-\gamma}\ (\gamma = x/2 - y/2).$$

Thus, the total number of oxygen vacancies is $\gamma = x/2 - y/2 = (x-y)/2$. As a result, taking into account the electroneutrality condition, the crystal chemical formula of $La_{1-x}Sr_xFeO_{3-\gamma}$ can be represented as:

$$La^{3+}_{1-x}Sr^{2+}_{x}Fe^{3+}_{1-y}Fe^{4+}_{y}O^{2-}_{3-\gamma} \Rightarrow$$
$$\Rightarrow (La^{3+}_{1-x}Sr^{2+}_{x})(Fe^{3+}_{1-x+2\gamma}Fe^{4+}_{x-2\gamma})(O^{2-}_{3-\gamma}\square_{\gamma}), \qquad (1)$$

where $x, y = x-2\gamma$ and $\gamma = (x-y)/2$ are the numbers of Sr^{2+}, Fe^{4+} ions and oxygen vacancies ($\square$) per formula unit of ferrite, respectively. Then, the number of oxygen ions in a substituted ferrite can conditionally be represented in the form of two parts. One part is „base"; the number of such oxygen ions depends on the La/Sr ratio. The second part is „variable", which in this scheme is associated with the presence of a Fe ion — an element with variable valence. Vacuum annealing can reduce the number of oxygen ions to the limiting value $(3-x/2)$. In this case, accordingly, Fe^{4+} transfers to Fe^{3+}. As a result, it can be concluded that the as−prepared samples of substituted lanthanum ferrites have base oxygen, variable oxygen, as well as Fe^{4+} and Fe^{3+} ions. The samples annealed in vacuum at 650°C have only base oxygen and Fe^{3+} ions. Tables 2 and 3 summarize all the parameters obtained from the analysis of the Mössbauer results for the compounds considered.

3.4. Magnetic data

The substituted $La_{1-x}Sr_xFeO_{3-\gamma}$ is antiferromagnetic orthoferrite [4,15] the same as $LaFeO_3$ ($T_N = 740$ K [24]) and $SrFeO_3$ ($T_N = 134$ K [25]).

Figure 6 illustrate the temperature dependencies of magnetization $M(T)$ measured in the ZFC and FC modes (the sample is pre-cooled in zero field cooling and field cooling at $H = 10$ kOe), and magnetic field strength $M(H)$ of the as−prepared Sr50 and Sr33 samples. In general, the behavior of these dependencies for the Sr50 and Sr33 samples is similar. The paramagnetic nature of the as−prepared Sr50 sample at room temperature is confirmed by the linear $M(H)$ dependence at $T = 300$ K (Figure 6, *b*). The type of the $M(H)$ dependence for paramagnets depends on the temperature at which the measurements were carried out. At low temperatures, the $M(H)$ curve of paramagnets is described by the Brillouin function, when $gS\mu_BH/k_BT \gg 1$. At high temperatures, as in our case, the Brillouin function degenerates into a straight line, when $gS\mu_BH/k_BT \ll 1$ (Figure 6, *b*). At $T = 2$ K, the $M(H)$ curve of the Sr50 sample does not described by the Brillouin function and demonstrates a hysteresis that corresponds to the magnetically ordered state such as weak ferromagnetism rather than paramagnetic one.

For the Sr50 and Sr33 samples, several characteristic temperatures are observed on the $M(T)$ curves (Figures 6, *a* and 7, *a*). However in the frame of this work, the main interest is the Néel temperatures T_N, the effect of the Sr concentration on them, the number of Fe^{4+} ions and oxygen ions. In the Sr50 sample, the temperature $T_N \approx 233$ K corresponds to the inflection of both $M(T)$ curves (Figure 6, *a*) and is clearly visualized by the dM/dT derivative. The temperature T_N for the Sr33 sample (Figure 7, *a*) is obtained by approximating the curve in the vicinity of a transition to the magnetically ordered state and is ≈ 385 K. The FC−ZFC curves begin to diverge below T_N for both samples.

In the Sr33 sample (Figure 7, *b*) that is magnetically ordered at room temperature, the hysteresis loop disappears at ~ 400 K, and the $M(H)$ curve becomes linear.

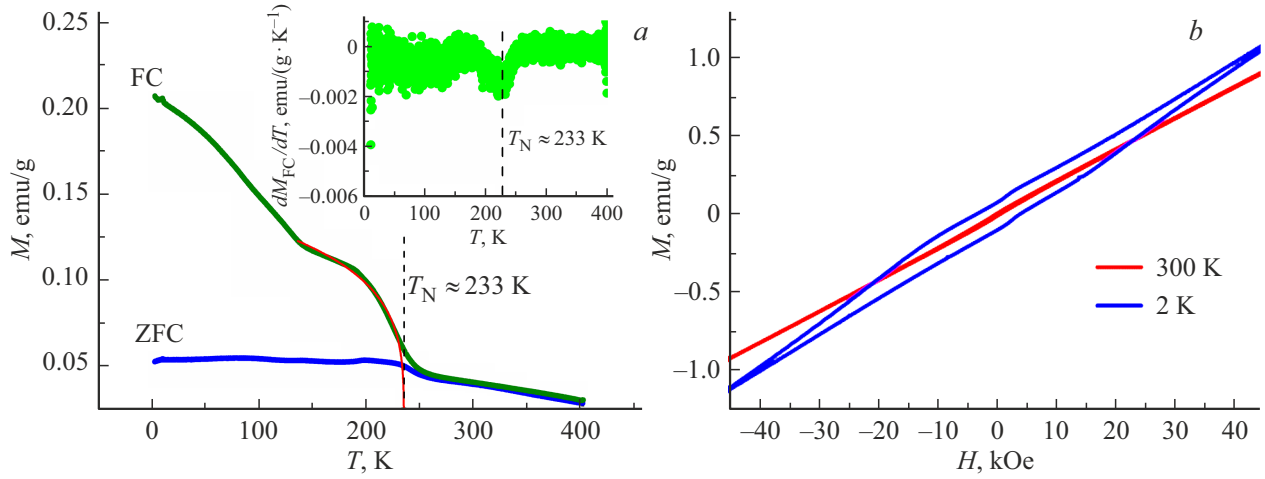

Figure 6. (*a*) The temperature dependencies of magnetization $M(T)$ measured in the ZFC and FC modes of the as−prepared Sr50 sample. Red line is an approximation of the vicinity of a transition to the magnetically ordered state. dM_{FC}/dT is shown in the insert. (*b*) Magnetic hysteresis loops measured at temperatures of $T = 2$ and 300 K.

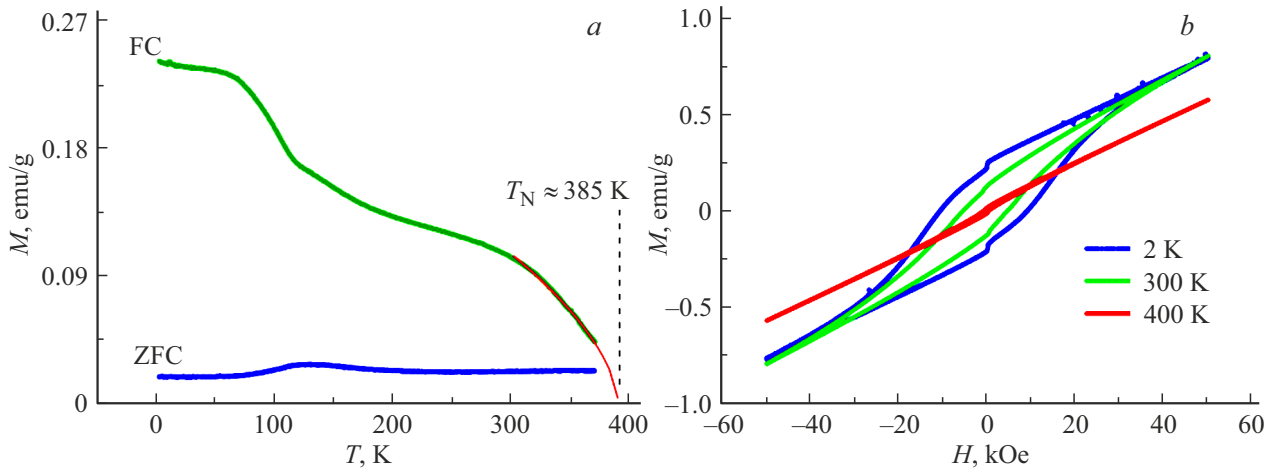

Figure 7. (*a*) The temperature dependencies of magnetization $M(T)$ measured in the ZFC and FC modes of the as−prepared Sr33 sample. Red line is an approximation of the vicinity of a transition to the magnetically ordered state. (*b*) Magnetic hysteresis loops measured at different temperatures.

Similar curves were previously observed in substituted $La_{1-x}Sr_xFeO_{3-\delta}$ orthoferrites with $x = 2/3$ and 3/4 with an antiferromagnetic structure [26]. The spins in them are aligned antiparallel due to an antiferromagnetic bond between two neighboring Fe^{3+} ions through an intermediate oxygen ion. A slight deviation of spins from a strict antiparallel orientation, which results from a zigzag arrangement along the c axis of oxygen octahedra containing Fe ions, leads to the emergence of weak („parasitic“) ferromagnetism in the samples [26]. Indeed, a significant ferromagnetic component is observed on the $M(T)$ curves, which is described near the temperature of a transition to the magnetically ordered state by the function $M(T) \sim (T_N - T)^{\beta}$ with $T_N \approx 233$ K for the Sr50 sample (Figure 6, *a*) and $T_N \approx 385$ K for the Sr33 sample (Figure 7, *a*). In classical collinear antiferromagnets, the temperature dependence of magnetization passes through a maximum corresponding to T_N. This happens since the antiparallel ordering of the spins is gradually disrupted with an increase in the temperature, and in contrast to the paramagnet, the total magnetization increases. The antiparallel spin ordering disappears above T_N, and spin disorder is formed. Therefore, the magnetization begins to decrease with a further increase in the temperature, like in the paramagnet. The temperature dependence of magnetization for weak ferromagnets is similar to that for ordinary ferromagnets, i. e., it increases monotonically with a decrease in the temperature, shows no maximum, and disappears at T_N as observed in our samples. The difference is that the magnetization value does not exceed a few percent of the case if the ferromagnetic order were in the substance. The presence of ferromagnetism is

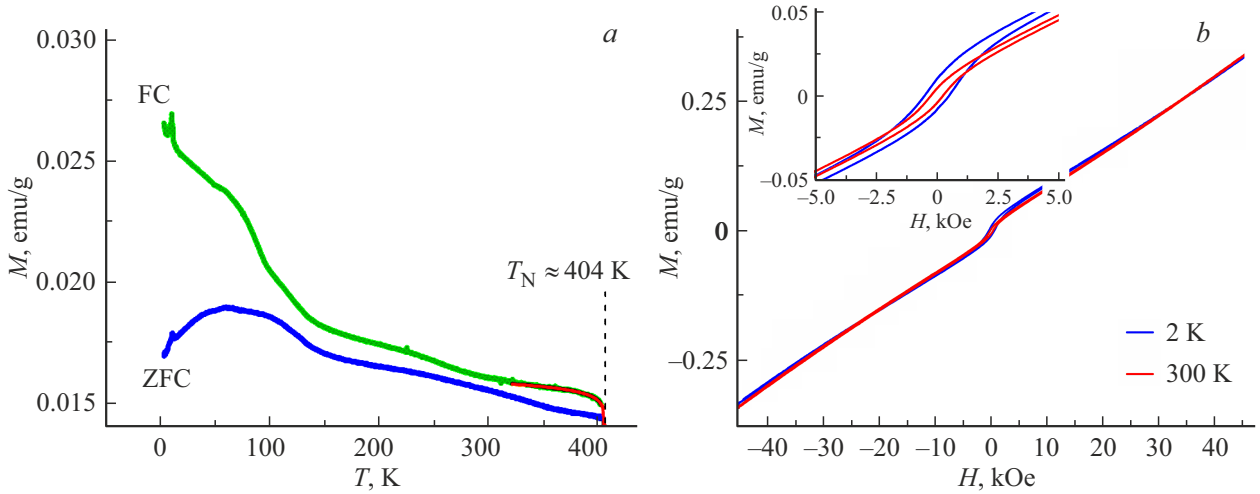

Figure 8. (a) The temperature dependencies of magnetization $M(T)$ measured in the ZFC and FC modes of the Sr50 sample annealed at 650°C. Red line is an approximation of the vicinity of a transition to the magnetically ordered state. (b) Magnetic hysteresis loops measured at temperatures of 2 and 300 K. The low-field loops fragment is shown in the insert.

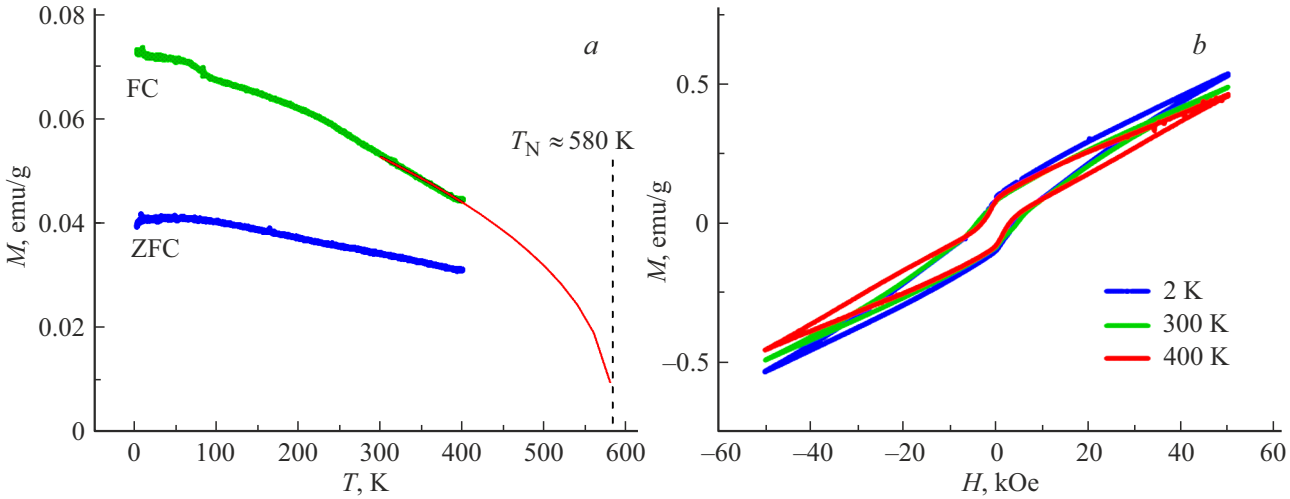

Figure 9. (a) The temperature dependencies of magnetization $M(T)$ measured in the ZFC and FC modes of the Sr33 sample annealed at 650°C. Red line is an approximation of the vicinity of a transition to the magnetically ordered state. (b) Magnetic hysteresis loops measured at different temperatures.

also confirmed by hysteresis in the $M(H)$ curves, which are generally linear and characteristic of antiferromagnets (Figures 6, b and 7, b). The $M(H)$ dependence in antiferromagnets has a linear form in not very strong magnetic fields (strong magnetic fields destroy the antiferromagnetic order). This agrees well with the data from [27].

The summary data on T_N for all as−prepared samples and those annealed in vacuum at 650°C are listed in Table 4.

As shown above, the fraction of Fe^{4+} in the mixture of Fe^{4+} and Fe^{3+} ions increases with an increase in the ion substitution of Sr^{2+} for La^{3+}, which leads to an increase in the number of ferromagnetic interaction channels due to the double exchange $Fe^{4+}-Fe^{3+}$ [28], and a decrease in the number of antiferromagnetic exchange channels $Fe^{3+}-Fe^{3+}$. Thus, the increase in the number of Sr ions leads to the redistribution of the contributions of ferro — (J_F) and antiferromagnetic (J_{AF}) channels into the resulting exchange and the shift of balance towards weakening antiferromagnetism. As a result, the magnetic ordering temperature T_N decreases from 385 K (the Sr33 sample, Figure 8, a) to 233 K (the Sr50 sample, Figure 6, a) with an increase in the Sr concentration.

The $M(T)$ curves measured in the ZFC and FC modes, and the $M(H)$ curves of the Sr50 and Sr33 samples after vacuum annealing at 650°C are shown in Figures 8 and 9. In general, the nature of these curves is similar to that observed in the as−prepared samples. The data for the Sr50 sample were taken from our previous work [29].

However, some changes occur under vacuum annealing. The temperature T_N corresponding to the point of inflection

Table 4. The summary data on T_N for the as−prepared samples and those annealed in vacuum at 650°C

Sample	Sr50, before annealing	Sr33, before annealing	Sr50, after annealing	Sr33, after annealing
T_N, K	233	385	404	580

and divergence of the FC−ZFC curves noticeably exceeds room temperature in the Sr50 sample and is significantly higher than 400 K in the Sr33 sample (Figure 9, *a*). This means that annealing leads to a significant increase in T_N of the Sr50 and Sr33 compounds, which still remain in the magnetically ordered state at room temperature (the Sr50 sample) and at 400 K (the Sr33 sample). This state is described by the function $M(T) \sim (T_N \sim T)^\beta$ with $T_N \approx 404$ K for the Sr50 sample (Figure 8, *a*) and $T_N \approx 580$ K for the Sr33 sample (Figure 9, *a*) near the temperature of a transition to the magnetically ordered state. This fact is confirmed by the presence of magnetic hysteresis loops at room temperature for the Sr50 sample (Figure 8, *b*) and at 400 K for the Sr33 sample (Figure 9, *b*).

As mentioned above, two interrelated processes occur in the crystal lattice under vacuum annealing: an oxygen ion is removed with the formation of a vacancy, and the valence state of Fe ions changes from 4+ to 3+. With an increase in the annealing temperature, the contributions of Fe^{3+} ions with different local environments are redistributed. The contribution of Fe^{3+} ions with all six exchange bonds $Fe^{3+}-O^{2-}-Fe^{3+}$ increases significantly for the samples annealed in vacuum at 650°C as compared to the as−prepared samples: from 12% to ∼ 60% for the Sr50 sample and from 18% to 70% for the Sr33 sample. This results in the redistribution of the contributions of the ferro — (J_F) and antiferromagnetic (J_{AF}) channels to the resulting exchange.

The other features on the $M(T)$ curves of both annealed Sr50 and Sr33 samples are not observed at lower temperatures (Figure 8, *a* and 9, *a*). This is due to the absence of Fe^{4+} ions and the presence of Fe^{3+} only in the annealed samples. Therefore, the averaged valence state (associated with the transfer of electrons between Fe^{3+} and Fe^{4+} ions at room temperature) cannot be observed with a decrease in the temperature.

4. Conclusions

The analysis of the obtained experimental data on substituted $La_{1-x}Sr_xFeO_{3-\gamma}$ ($x = 0.33,\ 0.50$) makes it possible to draw the following conclusions.

– The unit cell volume decreases as the Sr concentration increases in both as−prepared samples and those annealed at 650°C. However, this decrease is weaker in the annealed samples.

– The number of Fe^{4+} ions in the as−prepared samples increases linearly with an increase in the Sr concentration.

– With an increase in the Sr concentration, the number of oxygen vacancies in the annealed samples increases faster than in the as−prepared ones.

– Most Fe^{3+} ions in the as−prepared samples (∼ 40% for the Sr33 sample and ∼ 35% for the Sr50 sample) have one or two defects in their local environment — a broken or a weakened bond. In the samples annealed at 650°C, Fe^{3+} ions dominate (∼ 70% for Sr33 and ∼ 60% for Sr50) which have an octahedral oxygen environment, i. e., all six superexchange bonds.

– The Néel temperatures T_N have been determined from the magnetic measurements. It was shown that as compared to the as−prepared samples, the redistribution of Fe^{3+} ions with different local environments under vacuum annealing resulted in a change of the J_F/J_{AF} ratio, a shift of the balance towards the increase in the antiferromagnetic order and a noticeable increase in T_N, as well as a decrease in the width of the magnetic hysteresis loops and the magnetization value.

– The magnetic measurements show a good correlation with the X-ray and Mössbauer data.

Acknowledgments

The authors are grateful to the Center for Collective Use of Scientific Equipment of the Osipyan Institute of Solid State Physics RAS for the experimental opportunities provided.

Funding

The work was carried out with the support of the Ministry of Science and Higher Education of the Russian Federation within the framework of the State assignments of the Federal Research Center for Problems of Chemical Physics and Medical Chemistry of the Russian Academy of Sciences (reg. number 124013100858-3) and the Osipyan Institute of Solid State Physics RAS.

Author statement

V. Sedykh: Supervision, Conceptualization, Investigation, Writing — Original Draft, Writing — Review & Editing, O. Rybchenko: Investigation, Formal analysis, Writing — Review & Editing, A. Dmitriev: Investigation, Formal analysis, Writing — Review & Editing, V. Kulakov: Formal Investigation, M. Gapochka: Investigation, V. Rusakov: Conceptualization, Writing — Original Draft.

Declaration of competing interest

The authors declare that they have no known competing financial interests or personal relationships that could have appeared to influence the work reported in this paper.

References

[1] S. Petrovic, A. Terlecki, L. Karanovic, P. Kirilov-Stefanov, M. Zduji, V. Dondur, D. Paneva, I. Mitov, V. Rakic. Appl. Catal. B Environ. **79**, 186 (2008). https://doi.org/10.1016/J.APCATB.2007.10.022.

[2] J. Faye, A. Bayleta, M. Trentesauxb, S. Royera, F. Dumeignil, D. Duprez, S. Valange. Appl. Catal. B Environ. **126**, 134 (2012). https://doi.org/10.1016/J.APCATB.2012.07.001.

[3] E.K. Abdel-Khalek, D.A. Rayan, Ahmed. A. Askar, M.I.A. Abdel Maksoud, H.H. El-Bahnasawy. J. Sol-Gel Sci. and Technology **97**, 27 (2021). https://doi.org/10.1007/s10971-020-05431-8.

[4] J.B. Yang, W.B. Yelon, W.J. James, Z.Chu, M. Kornecki, Y.X. Xie, X.D. Zhou, H.U. Anderson, Amish G. Joshi, S.K. Malik. Phys. Rev. B **66**, 184415 (2002). https://doi.org/10.1103/PhysRevB.66.184415.

[5] V.D. Sedykh, O.G. Rybchenko, A.N. Nekrasov, I.E. Koneva, V.I. Kulakov. Phys. Solid State **61** (6), 1099 (2019). DOI: 10.1134/S1063783419060210.

[6] V.D. Sedykh, O.G. Rybchenko, E.V. Suvorov, A.I. Ivanov, V.I. Kulakov. Phys. Solid State **62** (10), 1916 (2020). DOI: 10.1134/S1063783420100297.

[7] V.D. Sedykh, O.G. Rybchenko, N.V. Barkovskii, A.I. Ivanov, V.I. Kulakov. Phys. Solid State **63** (12), 1775 (2021). DOI: 10.1134/S1063783421100322.

[8] O.I. Barkalov, S.V. Zaitsev, V.D. Sedykh. Solid State Commun. **354**, 114912 (2022). https://doi.org/10.1016/j.ssc.2022.114912.

[9] V. Sedykh, O. Rybchenko, V. Rusakov, S. Zaitsev, O. Barkalov, E. Postnova, T. Gubaidulina, D. Pchelina, V. Kulakov. J. Phys. Chem. Solids **171**, 111001 (2022). https://doi.org/10.1016/j.jpcs.2022.111001.

[10] V. Sedykh, V. Rusakov, T. Gubaidulina. Phys. Solid State **65** (4), 613 (2023). DOI: 10.21883/PSS.2023.04.56003.18.

[11] V.D. Sedykh, V.S. Rusakov, T.V. Gubaidulina, O.G. Rybchenko, V.I. Kulakov. PMM **124** (2), 153 (2023). DOI: 10.1134/S0031918X22601950.

[12] V. Sedykh, V. Rusakov, O. Rybchenko, A. Gapochka, K. Gavrilicheva, O. Barkalov, S. Zaitsev, V. Kulakov. Ceramics Intern. **49** (15), 25640 (2023). https://doi.org/10.1016/j.ceramint.2023.05.105.

[13] J.B. Goodenough. Metallic oxides, in Progress in Solid State Chemistry, edited by H. Reiss (Pergamon, London, **5** (1971) 145−399. https://doi.org/10.1016/0079-6786(71)90018-5.

[14] J.B. Goodenough, in Magnetism and Chemical Bond, edited by F. Albert Cotton (Interscience, London, **1** (1963) 154.

[15] J. Grenier, N. Ea, M. Pouchard, M.M. Abou-Sekkina. Mater. Res. Bull. **19**, 1301 (1984). https://doi.org/10.1016/0025-5408(84)90192-2.

[16] P.D. Battle, N.C. Gibb, S. Nixon. J. Solid State Chem. **79**, 75 (1989). https://doi.org/10.1016/0022-4596(89)90252-1.

[17] M.E. Matsnev, V.S. Rusakov. AIP Conf. Proc., American Institute of Physics AIP, **1489**, 178 (2012). https://doi.org/10.1063/1.4759488.

[18] P.D. Battle, T.C. Gibb, S. Nixon. J. Solid State Chem. **77**, 124 (1988). https://doi.org/10.1016/0022-4596(88)90099-0.

[19] G. Li, L. Li, M. Zhao. Phys. Stat. Sol. B **197**, 165 (1996). https://doi.org/10.1002/pssb.2221970123

[20] Y. Shin, K.-Y. Doh, S.H. Kim, J.H. Lee, H. Bae, S.-J. Song, D. Lee. J. Mater. Chem. A **8**, 4784 (2020). DOI: 10.1039/c9ta12734h.

[21] G.A. Sawatzky, F. van der Woude. J. Phys. Colloq. **35**, 47 (1974). https://doi.org/10.1051/jphyscol:1974605.

[22] V.I. Nikolaev, V.S. Rusakov, Mossbauer Studies of ferrites, Moscow State University, Moscow, 1985 (in Russian)

[23] T.M. Rearick, G.L. Catchen, J.M. Adams. Phys. Rev. B **48**, 224 (1993), https://doi.org/10.1103/PhysRevB.48.224.

[24] P.K. Gallagher, J.B. MacChesney, D.N.E. Buchanan. J. Chem. Phys. **41**, 2429 (1964), https://doi.org/10.1063/ 1.1726282.

[25] J. Blasco, B. Aznar, J. García, G. Subías, J. Herrero-Martín, J. Stankiewicz. Phys. Rev. B **77** (5) (2008). https://doi:10.1103/physrevb.77.054107

[26] U. Shimony, J.M. Knudsen, Mossbauer Studies on Iron in the Perovskites $La_{1-x}Sr_xFeO_3$ $(0 \leq x \leq l)$. Phys. Rev. **144** (1) (1966) 361−366.

[27] I. Zvereva, T. Pavlova, V. Pantchuk, V. Semenov, Y. Breard, J. Choisnet. Chimica Techno Acta **1**, 46 (2016). DOI: 10.15826/chimtech.2016.3.1.004.

[28] A.I. Dmitriev, S.V.Zaitsev, M.S. Dmitrieva, O.G. Rybchenko, V.D. Sedykh. Phys. Solid State **66** (3), 386 (2024). DOI: 10.61011/FTT.2024.03.57479.1 (in Russian).